Distribution Category:
LMFBR--Components: Base
Technology (UC-79k)

ANL-86-11

ANL--86-11

DE86 010765

ARGONNE NATIONAL LABORATORY
9700 South Cass Avenue
Argonne, Illinois 60439

LEAKAGE FLOW-INDUCED VIBRATIONS FOR VARIATIONS OF A TUBE-IN-TUBE SLIP JOINT

by

T. M. Mulcahy

Components Technology Division

DISCLAIMER

January 1986

CONTENTS

FIGURES

TABLES

NOMENCLATURE

D	Inside diameter of slip joint annular constriction
BL	Length of bevel
EC	Eccentricity of tubes
f	Modal frequency
IL	Engagement length of tubes
L	Length of constriction annulus
LD	Length of annulus between tubes
M	Modal mass
R	Mean radius of fluid-filled annulus between tubes
V	Average velocity in the annular constriction
W	Radial gap between concentric tubes
W'	Radial gap of annular constriction for concentric tubes
ΔP	Pressure drop across the slip joint
ζ	Modal damping (% of critical damping)
ζ_o	Modal damping with no flow
ρ	Fluid mass density

LEAKAGE FLOW-INDUCED VIBRATION FOR VARIATIONS OF A TUBE-IN-TUBE SLIP JOINT

by

T. M. Mulcahy

ABSTRACT

Variations in the design of a specific slip joint separating two cantilevered, telescoping tubes conveying water were studied to determine their effect upon the leakage flow-induced vibration self-excitation mechanism known to exist for the original slip joint geometry. The important parameters controlling the self-excitation mechanism were identified, which, along with previous results, allowed the determination of a comprehensive set of design rules to avoid unstable vibrations. This was possible even though a new self-excitation mechanism was found when the engagement of the two tubes was small.

I. INTRODUCTION

Main coolant flow paths through the components of a reactor system often parallel each other from one relatively constant-pressure, stagnant plenum region to another. However, the flow paths and plenum regions are rarely completely sealed from each other because of design requirements to allow for thermal expansion of components or their removal. Thus, leakage flow across pressure boundaries is not uncommon. When component vibration can interact and alter the leakage flow, the conditions for self-excited vibrations are present. Many reactor component designs have suffered from leakage flow-induced vibrations [1-3].

The avoidance of leakage flow-induced vibrations is difficult. Research to date shows that many excitation mechanisms can exist, depending on the local geometry of the leakage flow path, structural dynamics, and misalignment of components in the field. Rules-of-thumb for design exist [2], and unstable configurations often can be identified by analytical predictions. But the ability to quantitatively predict critical flowrates is very poor, and most commonly, suspect geometries are subject to extensive full-scale model testing.

Recently an experimental study was initiated [4] to gain a comprehensive understanding of the leakage flow excitation mechanisms associated with a specific tube-in-tube slip joint formed at the overlap of two cantilevered

tubes conveying fluid. The purpose of the continuing study is to understand the conditions for self-excitation so that at least one instability-free slip joint design can be defined for this common reactor structural configuration. The most recent testing concentrated on determining critical flowrates, flow damping, and pressure drops for the slip joint when the telescoping tubes were initially concentric [5] and eccentric [6]. Based on these results, design rules to avoid self-excitation were established for the specific tube-in-tube slip joint geometry shown in Fig. 1, defined in Table 1, and described further in Ref. 6. The design rules account for practical variations in some of the slip joint parameters, such as total engagement length IL, initial eccentricity of the tubes EC (0 to 100%), and damping ζ (0.5 to 6.0%) in the fundamental vibration mode. However, in the process of component design the need to vary other parameters can be expected. Thus, the sensitivity of the self-excitation mechanisms to variations in other parameters are reported here. In particular, the effect of changing the 30° entrance and exit bevels to the annular constriction, the length of the constriction L, and the constriction's radial gap W' were investigated.

II. ENTRANCE/EXIT BEVELS

The 30° entrance and exit bevels (conical convergences and divergences) of the slip joint of Fig. 1 were included in the original design for ease of engagement and disengagement of the two telescoping tubes [4]. They certainly were not included to provide a smooth flow transition to or from the narrow annular constriction of radial width W'. Flow separation is inevitable for such large angle diffusers and, in fact, self-excitation vibration mechanisms have been associated with the existence of such diffusers [2]. Thus, if design constraints permit, the elimination of the entrance and exit bevels from a design would not only reduce fabrication costs but possibly result in a better design for avoiding flow-induced vibrations.

To assess the effects of the removal of the entrance and exit bevels, slip joint configurations B (beveled) and D (square edge) (Fig. 2) were tested for the conditions of Table 2. Not all parameter variations previously studied [4-6] were tested here. Those included for testing were deemed sufficient to characterize the response for the conditions most likely to produce self-excitation. In particular, the eccentricity was maintained at EC ~ 0% (concentric), since previous test results [6] showed little sensitivity to eccentricity until EC approached 100% (tubes touching). Then, instabilities were less likely because of the increased initial (squeeze film) damping created by the close proximity of the tubes in the direction of the eccentricity. Also, testing was performed only with minimum (no flow) damping in the fundamental (f ~ 3.1 Hz) and second mode (f ~ 21.1 Hz) of the lower,

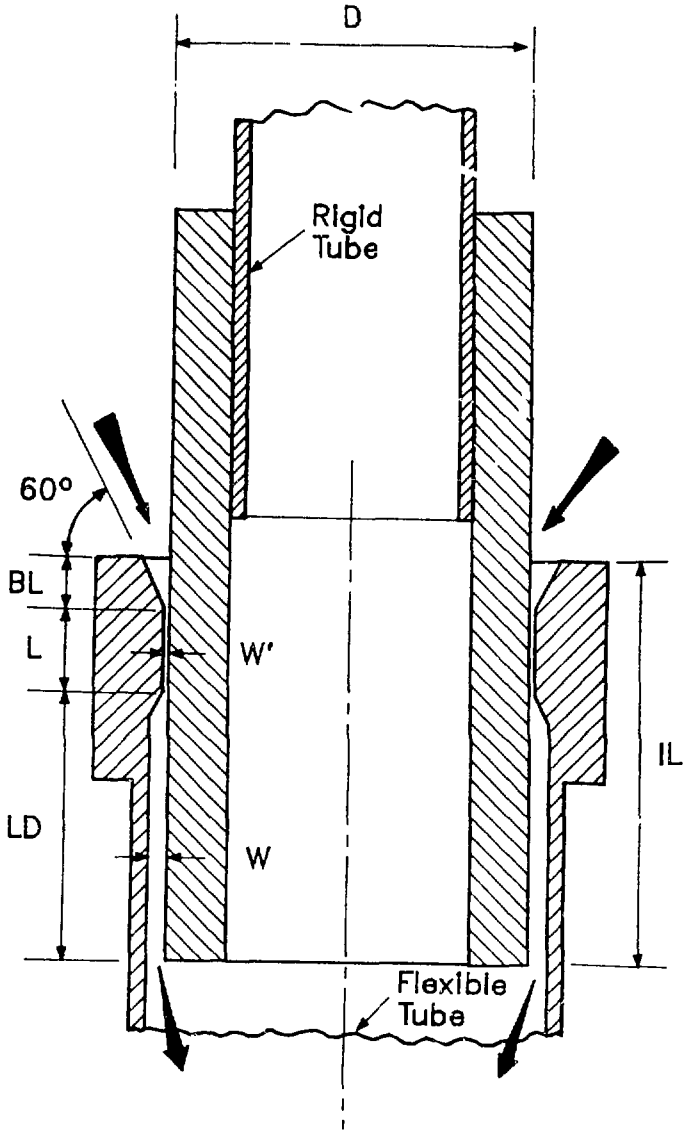

Fig. 1. Original Slip Joint

Table 1. Original Slip Joint Geometry

D = 5.0 in. (127 mm)	L = 0.20 D
W = 0.0562 D	IL = 0.30 to 1.0 D
W' = 0.008 D	BL = 0.5 L

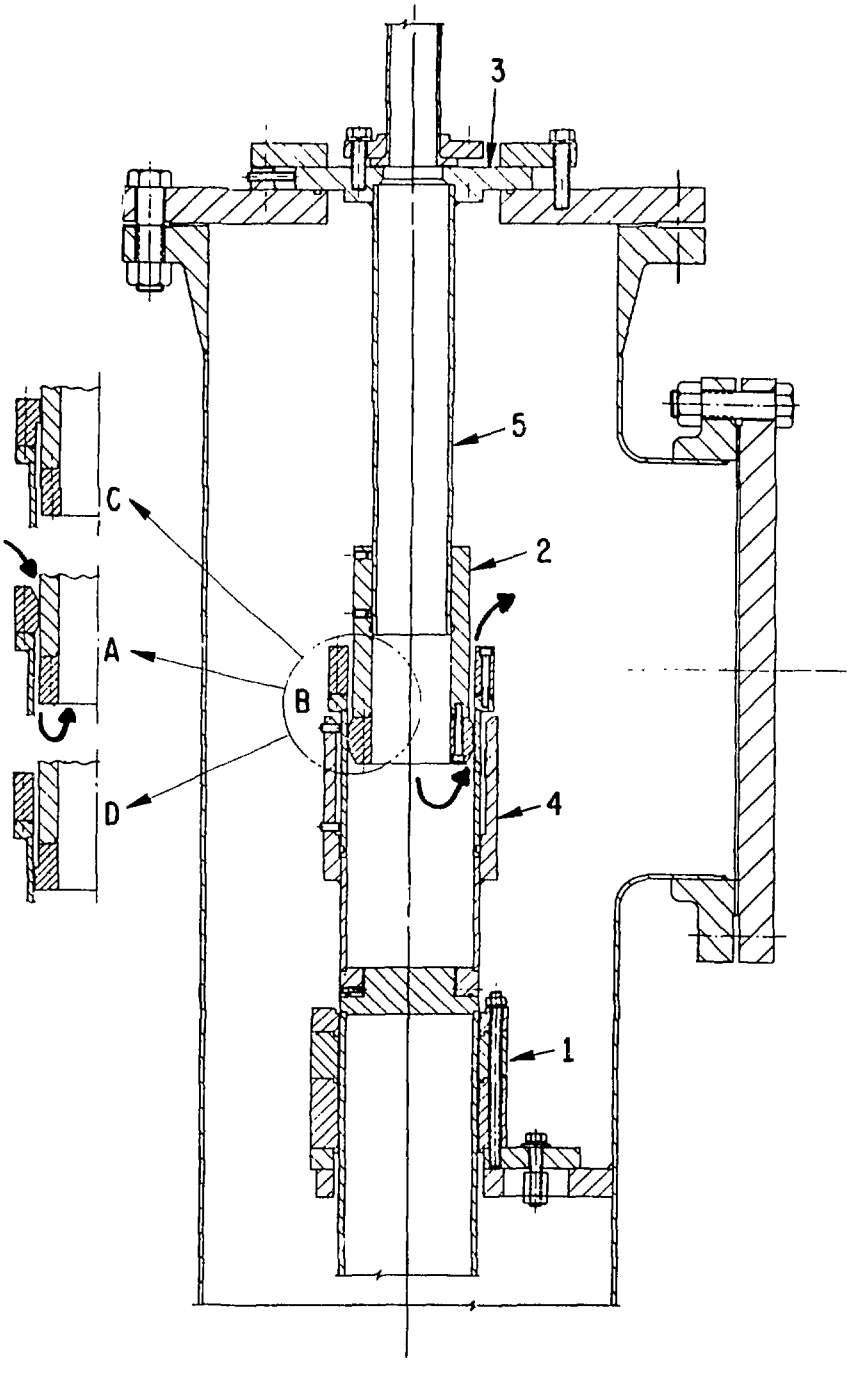

Fig. 2. Slip Joint Alternatives

Table 2. Entrance/Exit Bevel Assessment Geometry

D = 5.48 in. (139.2 mm)	L = 25.0 W'
W = 0.0513 D	IL = L→5L
W' = 0.142 W	LD = 0→4L

cantilevered tube: $\zeta_o \sim 0.5\%$ and 0.3%, respectively. The damping of the primarily translational motion of the fundamental mode at the slip joint could be increased, if desired, by adding squeeze film damping rings (item 1, Fig. 2) located near the top of the lower flexible tube. However, damping of the primarily rotational motion of the second mode at the slip joint was inherently structural, little affected by the squeeze film damping, and therefore not variable.

Testing with the flow in the direction shown in Fig. 2 produced upstream constrictions. The flow was reversed to produce downstream constrictions, but no self-excited vibration instabilities have been found, in past or present studies, for downstream constrictions. The response and self-excitation for upstream constrictions was observed for increasing flowrates, and damping was measured in the fundamental mode by pluck testing. Plots of damping versus flowrate have been found to be the best way to identify fundamental-mode critical flowrates--where self-excitation begins and the total modal damping is zero. Critical flowrates for self-excitation in the very lightly damped second mode could be visually identified without damping measurements, because the transition from forced to self-excited motion was very distinct. The details of the experimental flow facility, transducers, and testing procedures are described elsewhere [4-6].

The instability map for upstream beveled and square edge constrictions is shown in Fig. 3. The normalized reduced velocity V/2fW uses the average V in the narrow constriction of radial width W', and is plotted versus the normalized length of the annulus downstream from the constriction, LD/W. The open symbols represent fundamental-mode instabilities, while the solid denote second-mode instabilities. A slash through a symbol denotes the flowrate at which an instability ceased. Parameter values below or to the left of the solid line, a stability boundary, are not associated with self-excitation. Interestingly, the normalized critical velocity data points for both the beveled and square edge constrictions are almost indistinguishable from each other. Also, the critical values of the normalized velocity V/2fW are nearly the same whether the instability occurs in the first mode ($f \sim 3.1$ Hz) or the widely separated second mode ($f \sim 21.1$). Note that the no-flow damping in both modes is similar, $\zeta_o \sim 0.3$ versus 0.5%.

The choice of LD as the ordinate in Fig. 3, instead of the total engagement length IL, was based, in part, on the similarity of the damping curves for the same LD. Modal damping in the fundamental mode ζ_1, less the no flow value ζ_o, is shown in Fig. 4 for several LD and both types of upstream constrictions. The open symbols are for the beveled constriction while the solid are for the square edge one. The dotted portions of the curves, where $\zeta_1 - \zeta_o < 0$, indicate where an instability was initiated but ended at a higher

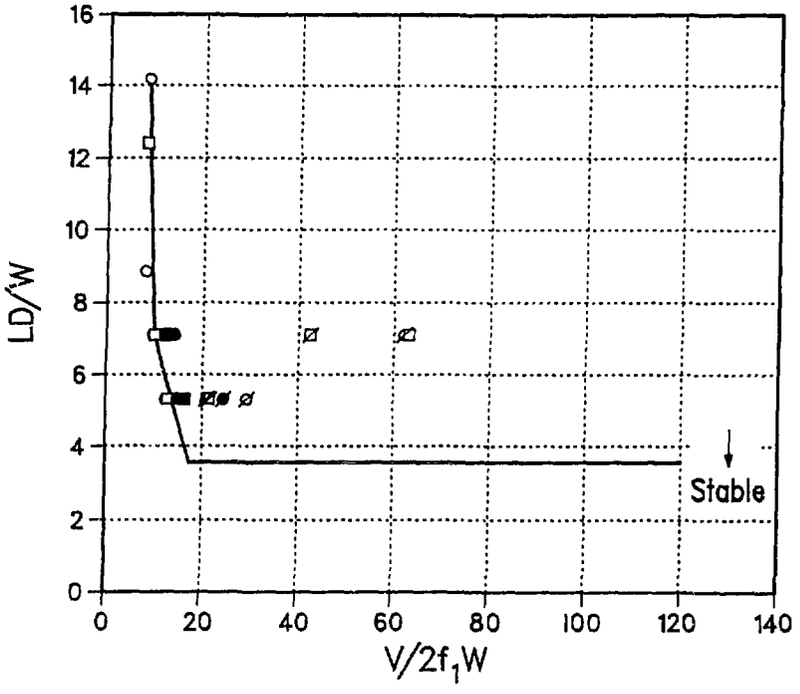

Fig. 3. Instability Map for Beveled (□) and Square-Edge (○) Constrictions with L/W' = 25.0, W/W' = 0.14, and Minimal Initial Damping

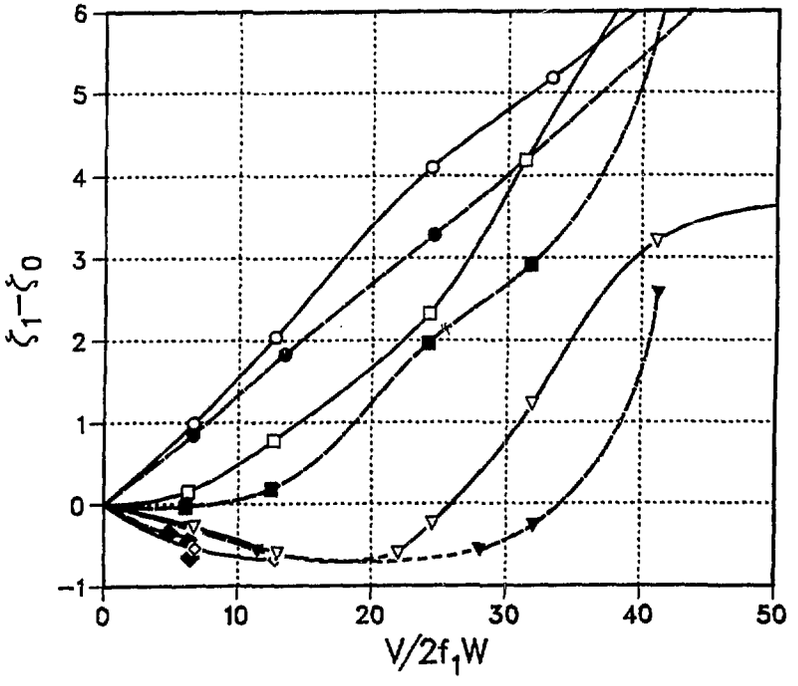

Fig. 4. Flow Damping for the Beveled and Square-Edge Upstream Constrictions with Several LD/W: 0.0, ○; 3.55, □; 5.32, ▽; and 7.09, ◇

flowrate. This borderline instability behavior occurred only for a narrow range of LD. In most cases, once the instability was initiated it did not disappear at higher flowrates (e.g., LD/W = 7.09).

Figure 5 shows that the damping curves for beveled and square **downstream** constrictions are similar to those for the upstream constriction. Also, as observed in past testing and shown in Fig. 5, the downstream constriction's flow damping monotonically increases with increases in LD.

Not surprisingly, the variation of the flexible tubes fundamental frequency and the pressure drop across the slip joint were similar for the beveled and square-edge constriction at the same flowrate. Compare (a) with (b) in Figs. 6 and 7. As in past testing, the pressure drop across the slip joint for a given flowrate was the same, regardless of flow direction (upstream or downstream constriction) or engagement lengths (again, the symbols are defined in Fig. 4).

III. SHORTER CONSTRICTIONS

Longer annular constrictions are more difficult to assemble and telescope, because exact parallel and concentric alignment is not possible in practice. One way to make the mechanical engagement easier is to shorten the constriction length L. To assess the effects of shortened constriction

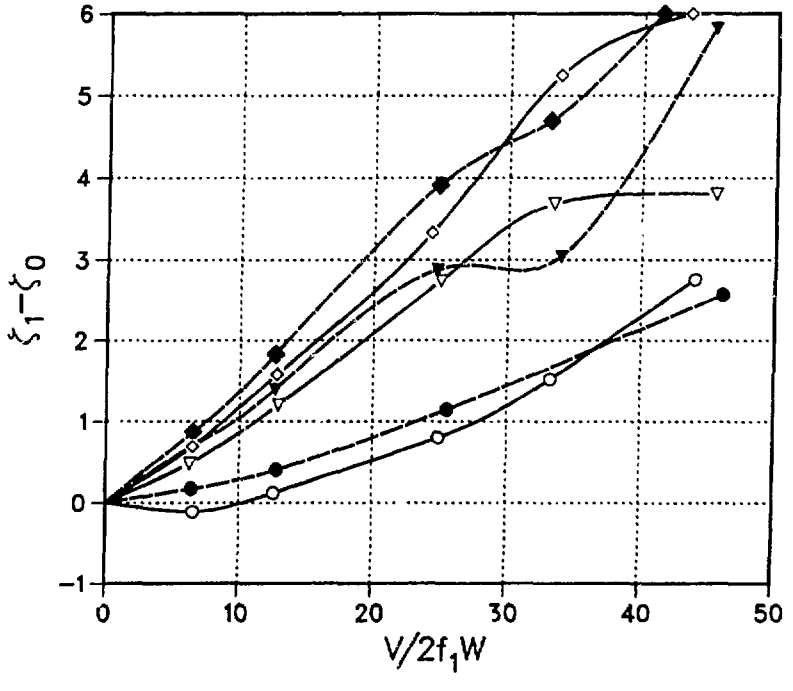

Fig. 5. Flow Damping When the Beveled and Square-Edge Constrictions are Downstream for the same LD/W of Fig. 4

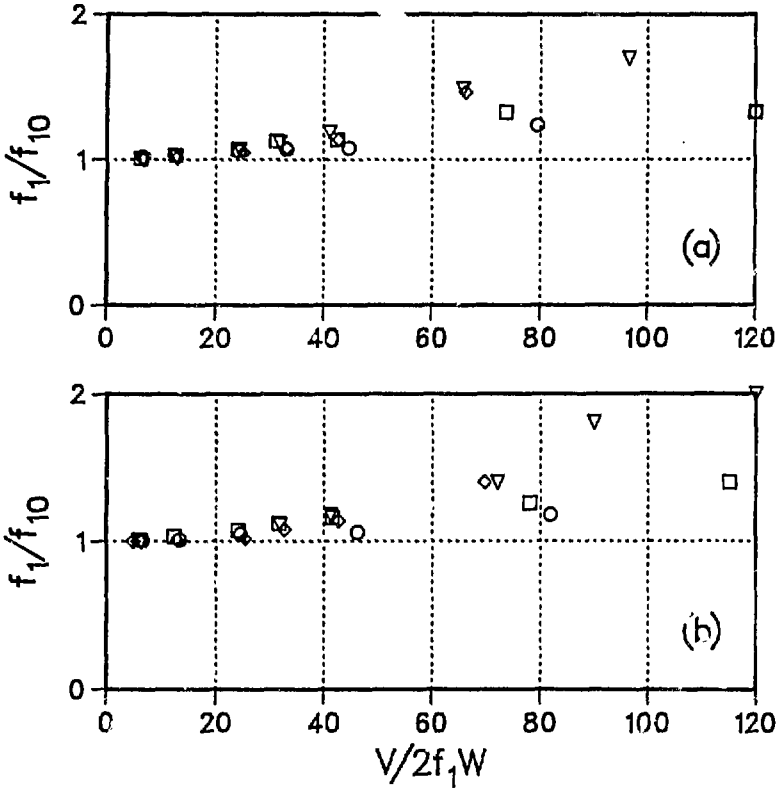

Fig. 6. Frequency Variation with Flow for the Upstream (a) Beveled Constriction and (b) Square-Edge Constriction

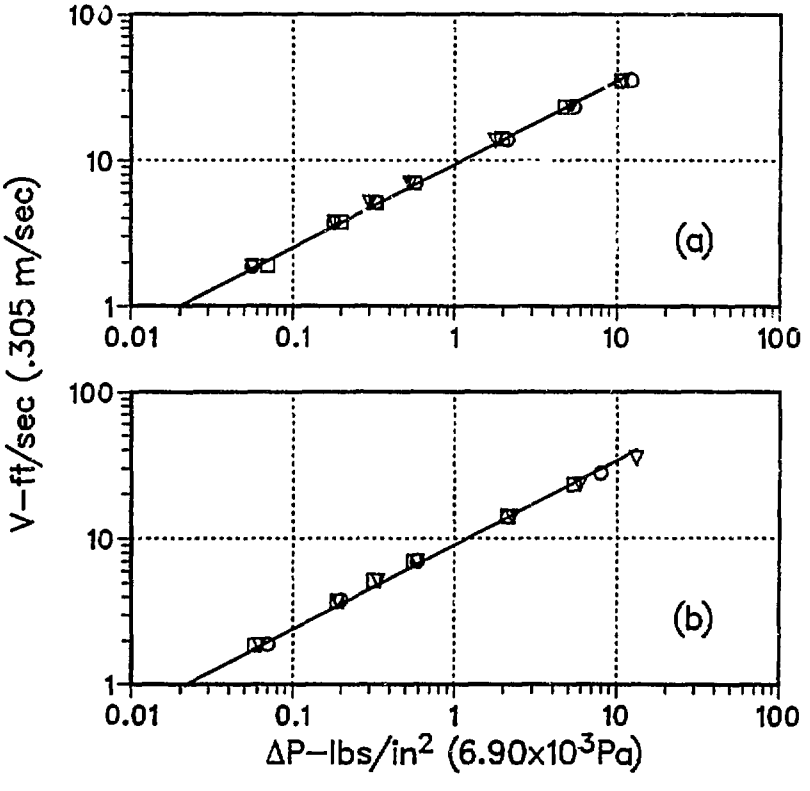

Fig. 7. Slip Joint Pressure Drop for (a) the Beveled and (b) the Square-Edge Constriction

lengths, two additional test series were performed with the square-edge constriction configuration D of Fig. 2. The same D, W, W', LD, ζ, and EC as used in the entrance/exit bevel assessment were tested with two constriction lengths, L = 12.5 W' and L = 6.25 W'. This allowed comparison of results at three constriction lengths for the same parameter variations, except for the engagement length IL. A choice had to be made between maintaining similar parameter variations for IL or LD. The downstream annulus length LD = IL - L was chosen because it was believed to be the more fundamental length parameter.

The instability map obtained is shown in Fig. 8. The open data points were obtained for an upstream constriction with the new constriction lengths, L = 12.5 W' and L = 6.25 W', while the solid curve is the same bounding curve for the L = 25.0 W' data shown in Fig. 3. The solid symbols are for downstream constrictions and will be discussed later. Obviously, there is little difference in the critical flow velocities for the different constriction lengths, especially when plotted versus LD/W, rather than IL/W. Surprisingly, no second-mode instability was observed for the shorter constriction lengths.

As might be expected for similar critical flow velocities, the flow damping shown in Fig. 9 was similar for all lengths of upstream constrictions with the same LD, if the LD was large enough to produce negative flow damping and self-excitation. The positive flow damping was not the same for the largest and intermediate-length upstream constrictions, L = 25.0 W' and

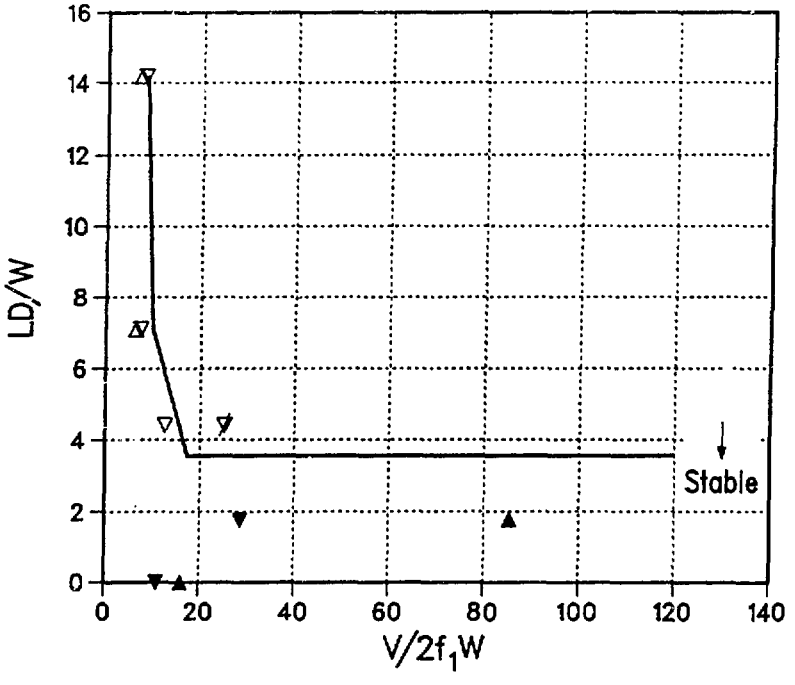

Fig. 8. Instability Map for the Square-Edge Constriction with Shorter L/W': 6.25, ∇ ; 12.5, Δ

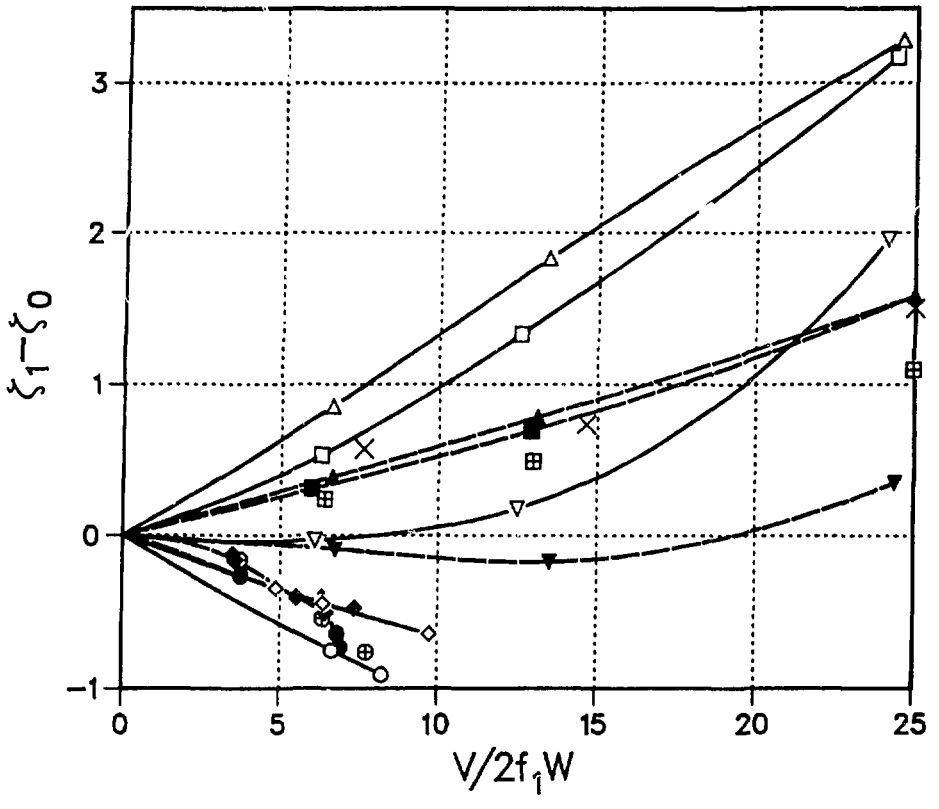

Fig. 9. Flow Damping for Different-Length Square-Edge, Upstream Constrictions. Open (——), Solid (---), and Crosshatched Symbols are for L/W' = 25.0, 12.5, and 6.25, respectively. (LD/W = 0.0, △; 1.77, □; 3.55, ▽; 7.09, ◇; 14.18, ○)

12.5 W'; at the same small LD, the longer L produced larger damping. Flow damping was similar for the intermediate and shortest-length upstream constrictions, L = 12.5 W' and 6.25 W. Figure 9 also includes another set of data taken to assess the choice of $\zeta_1 - \zeta_o$ as the ordinate variable. The data marked by x were taken for L/W' = 12.5 and LD/W = 0.0 at a large $\zeta_o \sim 3.3\%$ and they are seen to be similar to the data taken at a minimal $\zeta_o \sim 0.5\%$.

Fig. 10 shows that, within the accuracy of the pressure drop measurement, there was little difference between pressure drops when the constriction lengths were changed. The least square fit of the straight trend line in Fig. 10(a) for the longest constriction differs little from the trend line shown in Fig. 10(b) for the combined data of the intermediate and shortest constriction length. The curve fits for the longest and shortest constriction lengths are, respectively:

$$\ell n\ \Delta P = 2.04\ \ell n\ V - 4.48\ , \quad \text{and} \tag{1}$$

$$\ell n\ \Delta P = 2.11\ \ell n\ V - 4.85\ . \tag{2}$$

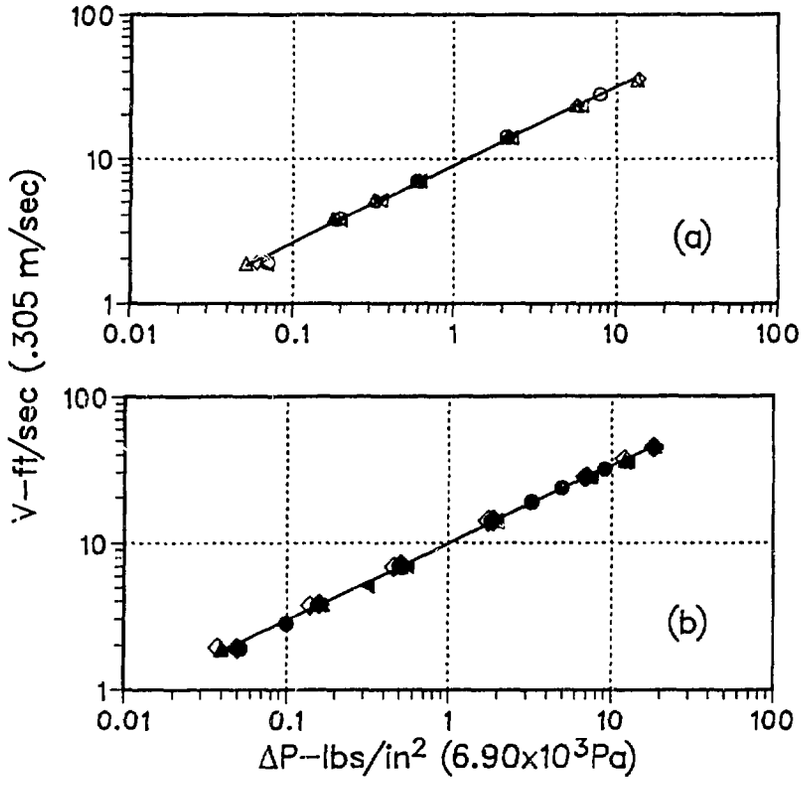

Fig. 10. Slip Joint Pressure Drop for the Square-Edge Constrictions with (a) L/W' = 25.0 and (b) L/W' = 12.5 (Solid Symbols), L/W' = 6.25 (Open Symbols). (LD/W = 0.0, ○; 1.77, ◁; 8.86, ◇; 14.18, △)

As before, the pressure drop data for the downstream constriction were similar to those for the upstream constriction. Evidently, the frictional losses produced along the length L of the narrow slip joint constriction were small compared with the sudden expansion and contraction losses at the entrance and exits of the constriction, at least for W'/W = 0.141.

Quite unexpectedly, testing of downstream constrictions with the shorter constriction lengths, L/W' = 12.5 and 6.25, revealed a new self-excitation mechanism that occurred only at very short engagement lengths (IL < 0.18 D = 25 W'). The critical velocities determined are shown by the solid symbols in Fig. 8. The instabilities were not as strong as those observed for an upstream constriction in the sense that the amplitude-limited unstable vibration did not increase as rapidly with increased flowrate, nor were the maximum amplitudes attained as large. Also, the mechanisms were strongest for the shortest engagement lengths (LD = 0.0 or IL = L), while they disappeared for engagements more than ~20% of the diameter. In contrast, instabilities associated with upstream constrictions were strongest for the largest engagement.

The flow damping curves shown in Figs. 11(a)-11(c) further illustrate the potential for self-excitation with a downstream constriction. Nearly the same negative damping was observed for the shortest and intermediate L = 6.25 W' and 12.5 W' at small LD/W = 0.0 and 1.77. But clearly, flow damping was always positive and significantly larger for L/W' = 25.0 at any LD $\gtrsim$ 0. Also, the flow damping was always positive, even at the shortest and intermediate L, when LD > 3.55 W ~ 0.2 D. However, note that IL becomes larger when LD is made larger, so there is no way to determine which of the two is the more important length parameter without further testing. Additional damping data, shown by the solid symbols, were obtained for larger ζ_o ~ 3.3% to assess the use of $\zeta_1 - \zeta_o$ as the ordinate parameter and extend the curve to larger $V/2f_1W$. Most of the data in Fig. 11 were obtained for damping of ζ_o ~ 0.5%. The data for the larger ζ_o appear to fall on the curve defined by the smaller ζ_o data, and obviously, the mechanism can be suppressed or moved to larger $V/2f_1W$ by increasing initial damping.

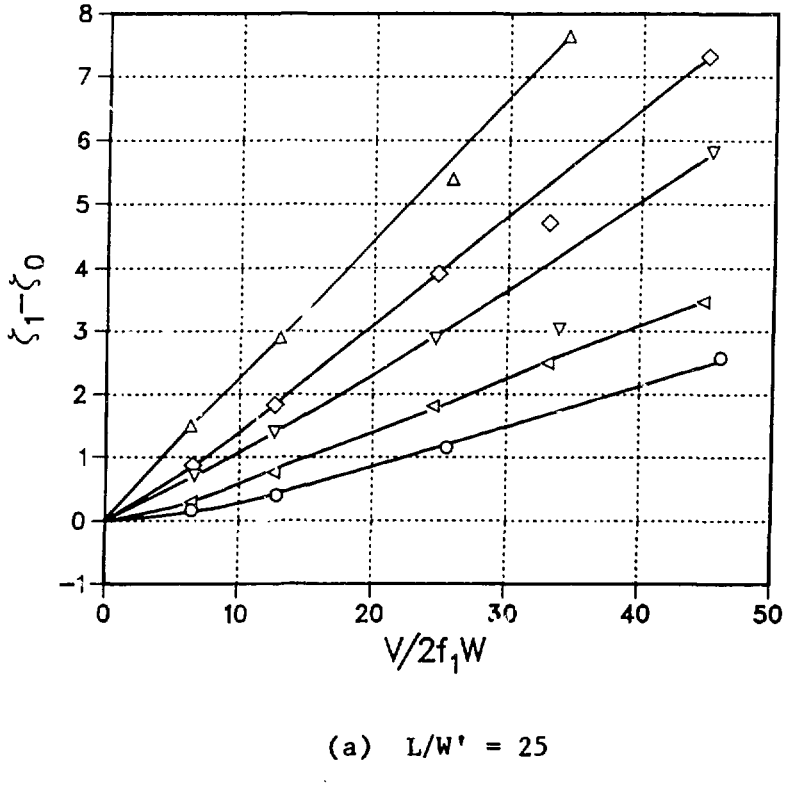

(a) L/W' = 25

Fig. 11. Flow Damping When the Square-Edge Constrictions are Downstream. (LD/W = 0.0, ○ ; 1.77; ◁ ; 3.55, □ ; 4.43, ▷ ; 5.32, ▽ ; 7.09, ◇ ; 14.18, △)

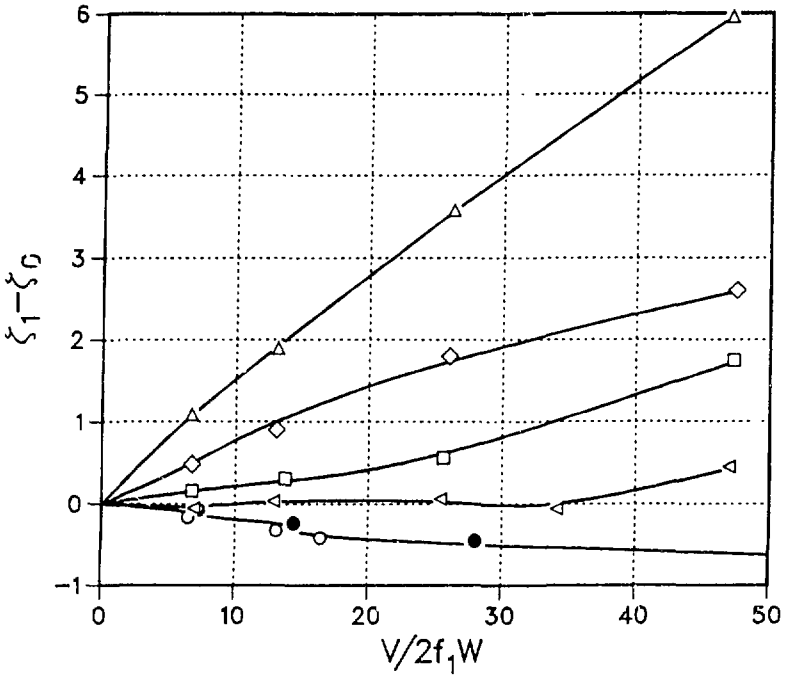

Fig. 11(b) L/W' = 12.5

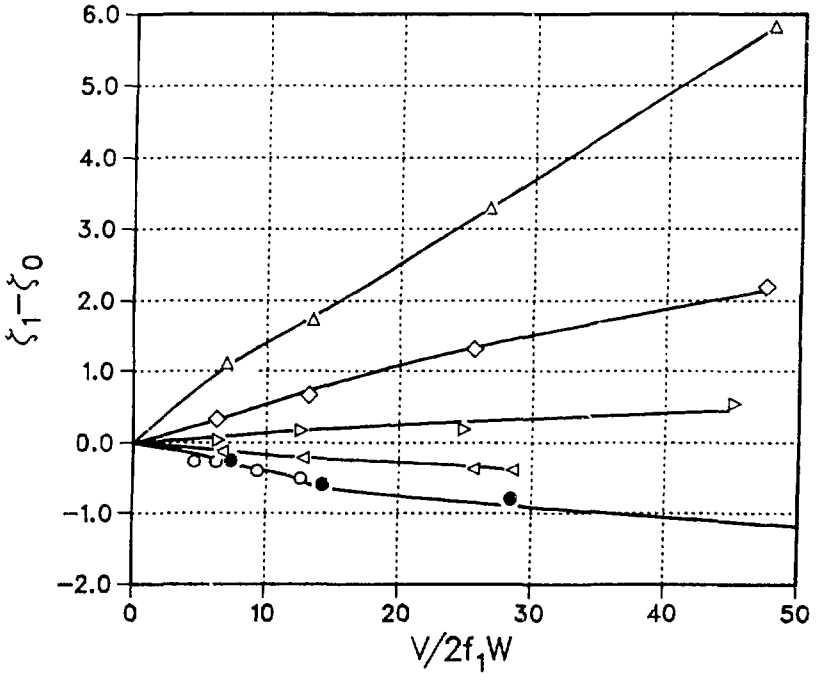

Fig. 11(c) L/W' = 6.25

IV. DIFFERENT ANNULAR GAPS

Perhaps the most likely design modification would be a change in the size of the narrow annular gap W'. The ability to assemble, telescope, or disassemble the slip joint is made easier by choosing larger values of W'. However, flow through the slip joint and the vibration of the tube due to forced excitation (e.g., turbulence) can be limited by using small W'. To further complicate the design choice, some test data [2] indicate that self-excited leakage flow vibrations might be eliminated if the constriction were made large enough $W'/W > 0.5$. Thus, a compromise W'/W is required.

To assess the effects of different annular gaps in an upstream constriction, additional tests were performed with $W'/W = 0.074, 0.14, 0.21, 0.29, 0.35, 0.49, 0.71, 1.0$. The square-edge configuration D in Fig. 2, with the shortest constriction length $L = 0.89$ W and minimum modal damping, was chosen for testing. It was the most susceptible to self-excitation of all previously tested upstream constriction configurations. The values of D, W, LD, ζ, and EC used previously were tested again.

The choice of the smallest value of W' to use in testing was dictated by the practical consideration that perfect alignment could not be realized. For D = 5.5 in. (139.7 mm) and L = 1.0 in. (25.4 mm), engagements without initial tube contact could not be set up unless $W' > 0.010$ in. (0.254 mm). This dictated the choice of $W'/W = 0.74$ as a lower limit. Of course, smaller W' could be set up without tube contact if the constriction length were limited to very short values, $L < 0.5$ in. (12.7 mm).

The instability map obtained for the short ($L/W = 0.89$) upstream constriction is shown in Fig. 12, where the critical velocities are plotted against W'/W, instead of LD/W as was done in Figs. 3 and 8. However, the length of the larger annulus LD is a parameter in the new map. For smaller W' or larger LD, the critical velocity $V/2f_1W$ for instability was lower. Also, for a given W', there existed a value of LD below which no instability occurred. These trends would be difficult to determine exactly without much more testing, but bounding relations were definable.

For purposes of design, solid lines were drawn on the instability map to identify parameter combinations free from self-excitation. For instance, regardless of LD/W, any combination of W'/W and V/2fW to the left of the angled solid lines are free from self-excitation. Combinations free from self-excitation also exist to the right of the angled solid line, if LD/W is small enough and W'/W large enough. For instance, if $LD/W < 3.6$, then self-excitation was not observed for any tested gap size, which included

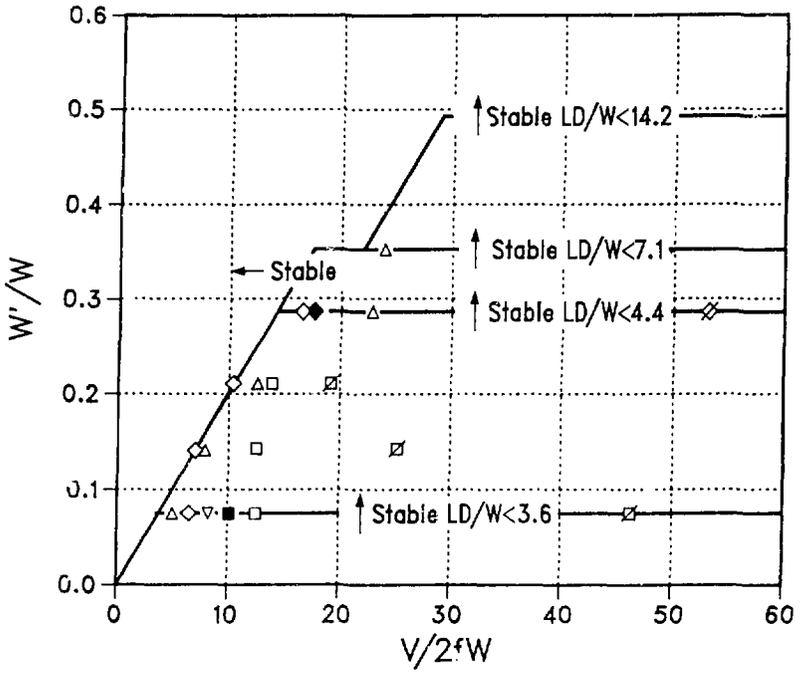

Fig. 12. Instability Map for the Shortest, Square-Edge Upstream Constrictions (L/W = 0.89) with Different W'/W. (LD/W: 4.43, □; 5.32, ▽; 7.09, ◇; 14.18, △)

W'/W ≥ 0.074; whereas, an LD/W > 7.1 would require W'/W ≥ 0.35 to avoid self-excitation. Finally, an upper bound of 0.5 on the gap size W'/W that will produce self-excitation does appear to exist, at least up to the maximum engagement length tested, LD/W = 14.2.

The complexity of the dependence of an upstream constriction's self-excitation on LD and W' is best seen in the three sets of damping curves shown in Fig. 13, which have been segregated according to LD/W = 1.77, 7.09, or 14.2. Several plots were attempted with different variables (e.g. ζ_1, V/2fW'), but $\zeta_1 - \zeta_o$ versus V/2fW grouped the trends together best. Even with these variables, maxima and inflection points can be observed in some of the curves. However, the curves in Fig. 13(c) clearly show that when LD is made sufficiently small, positive damping will be produced for any W'. In contrast, making LD larger does not guarantee that negative damping will be produced. One can see in Figs. 13(a)-(c) that W'/W between 0.35 and 0.5 appears to be the upper bound on constriction sizes that can produce negative damping and therefore be associated with a self-excitation mechanism.

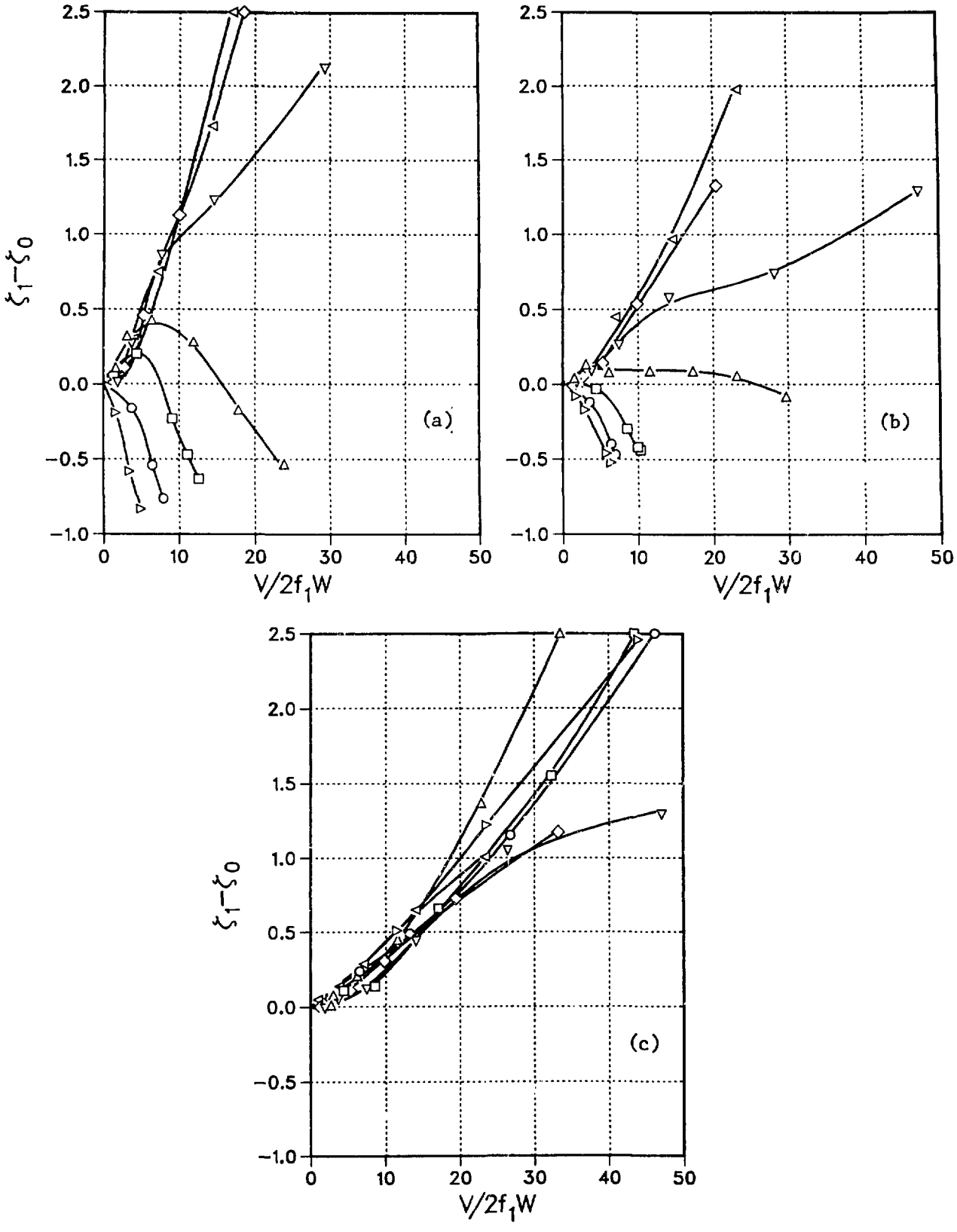

Fig. 13. Flow Damping When the Shortest Square-Edge Constrictions are Upstream. (a) LD/W = 14.18, (b) LD/W = 7.09, (c) LD/W = 1.77. (W/W' = 0.074, ▷; 0.14, ○; 0.21, □; 0.35, △; 0.50, ▽; 0.71, ◇; 1.0, ◁)

According to Fig. 13(a), there appeared to be no lower bound on the constriction size that would produce self-excitation nor the amount of negative damping that could be produced. However, as discussed previously, there was a lower bound as far as meaningful measurements were concerned. For $W'/W < 0.075$, assembly of the slip joint without producing contact, or even binding, between the tubes is difficult. In any case, the associated large frictional or impact damping makes the measurement of flow damping impossible. Therefore, the flow damping curve shown in Fig. 14, obtained for $W'/W = 0.074$ and $LD/W = 14.18$, represents the largest rate of negative damping that could be produced and measured within the limits of the test apparatus. To obtain the large negative values of damping (shown as solid symbols), an initial damping of $\zeta_o \sim 6.6\%$ was employed instead of $\zeta_o \sim 0.5\%$. The curve defined by $\zeta_o \sim 6.6\%$ appears to be a reasonable extension of $\zeta_o \sim 0.5\%$ curve. Note that the larger initial damping suppressed the self-excitation to significantly higher reduced velocities.

V. DISCUSSION

Variations in most of the design parameters of practical interest for the slip joint of Fig. 1 (L, W', LD or IL, BL, ζ_o, and EC) have been investigated for their effect on the self-excited vibrations of the lower flexible tube created by leakage flow through the slip joint at a constant pressure differential. The parameters held constant throughout testing were the ~ 2 ft (0.61 mm)-long rigid tube's outside diameter, D = 5.00 in. (127.0 mm), and the ~ 20 ft (6.1 m)-long flexible tube's inside diameter such that always W = 0.282 in. (7.16 mm). Also, the cantilevered supports of the tubes, opposite from the free ends that overlapped to form the slip joint, were never altered.

Since the tubes and their cantilevered supports were always the same, the only variations in the natural frequencies of the flexible tube for no flow were caused by changes in the engagement length IL or annular constriction gap size W' of the slip joint. Thus, the frequency of the fundamental mode, with primarily translational motion at the slip joint, was always different from test to test but in the range f = 2.7 to 3.1 Hz. The frequency of the second mode, with primarily rotational motion at the slip joint, was nearly always 21 Hz except when W' was very small or IL very long, at which point the frequency would shift to ~ 18 Hz. Essentially, the fluid confined in the annular regions of the slip joint produced significant added mass for translational motion but little for the rotational motion, except when the width/length of the annuli was small. Then the lower beam responded more as a fixed-hinged beam rather than a cantilevered beam. The fundamental frequency of the upper "rigid" tube was always ~ 85 Hz.

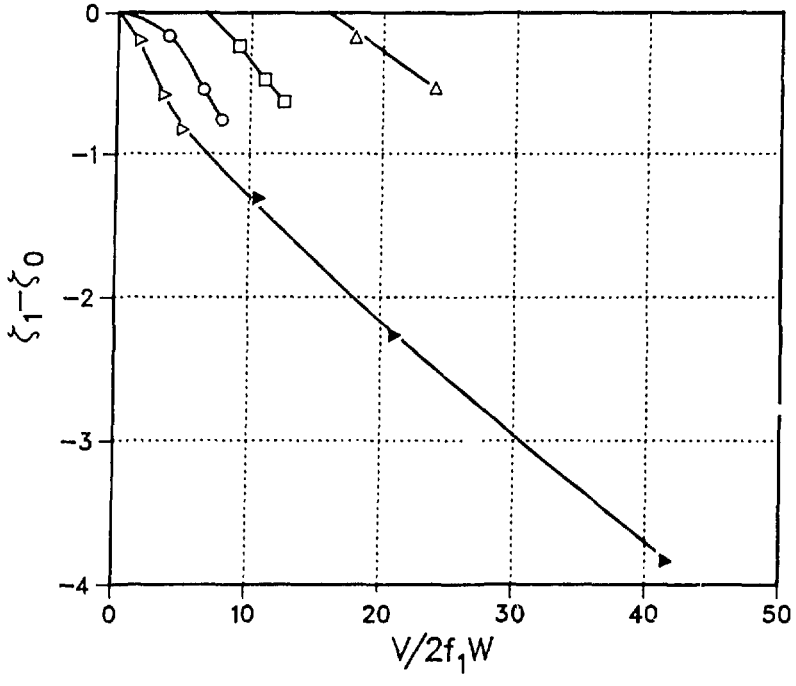

Fig. 14. Worst-Case Negative Damping Determined with $\zeta_o \sim 0.5\%$ and $\sim 6.6\%$ for a Square-Edge Upstream Constriction at L/W = 0.89, LD/W = 14.18, and W'/W = 0.074

A. An Upstream Constriction Mechanism

Two seemingly different self-excited vibration mechanisms were identified during testing. The strongest mechanism required the slip joint to have an upstream constriction and it occurred in both the first and second vibration modes for a wide range of the parameters. The flow directions of Figs. 1 and 2 all produce upstream constrictions for IL > L + BL or LD > 0. A physical explanation for such a mechanism has been identified for a sharp-edge constriction [2,7,8] and supported by data [5,8]. Since the bevels and length of the slip joint of Fig. 1 have been found to be irrelevant, the explanation for sharp-edge constriction mechanism is applicable. Essentially, the modulation and redistribution of the flow around the constriction annulus, caused by the alternate opening and closing of the constriction, creates a periodic pressure distribution and net force in the annulus downstream of the constriction that is in phase with the tube vibration velocity. When this negative flow damping is larger than the initial no-flow modal damping, then self-excitation will occur.

B. A Downstream Constriction Mechanism?

Since the other self-excitation mechanism was observed for case D in Fig. 2 with LD = 0.0, there is a question whether a constriction is necessary for the mechanism to exist. However, self-excitation was observed only when the flow was in the direction (outside to inside the tubes) that produces a downstream constriction for LD $\neq$ 0 and only in the fundamental mode. A physical explanation for this mechanism does not exist, nor have the parameters or the parameter ranges for which it exists been fully explored, as explained previously. Trends can be identified, however.

The flow damping appears to be measurable in terms of the same parameters used for the upstream constriction, $\zeta_1 - \zeta_o$ and $V/2f_1W$, as shown in Fig. 11. The excitation mechanism does appear to be a true self-excited instability, instead of forced excitation, because increased damping either completely suppressed the mechanism or moved its occurrence to a larger $V/2f_1W$. An important observation is that the potential for self-excitation becomes greater as the engagement length decreases, because the flow damping decreases. If the constriction length L and the engagement IL are small enough, negative damping is produced even when IL = L or LD = 0.0. It appears that a downstream constriction with sufficiently large LD or a sufficient constriction length provides a source of positive flow damping that suppresses a self-excitation mechanism that would otherwise exist at small IL. The governing length parameter for this mechanism is difficult to define with limited data. But we do know that this excitation mechanism occurs only for very short, impractical engagement lengths IL < 0.2 D, and, thus, is easily avoided in design. Accordingly, this mechanism is not discussed further here, but additional testing to understand and characterize the mechanism is planned.

C. Insignificant Design Variations

The upstream constriction mechanism was sensitive to only some of the parameter variations tested. As discussed in Section II, previous test results [6] showed that eccentricity of the tube did not change the critical velocities for upstream constrictions until the tubes were almost touching. Then the changes were attributed to increased initial damping caused by the squeeze film effect where the tubes were almost touching. Note that this insensitivity observation is limited to reduce velocities in the range tested $2 < V/2fW < 200$, and is probably related to the self-centering (static divergence) of the eccentric tubes with increased flow velocity. Thus, a dependence on eccentricity cannot be ruled out for stiffer systems with much smaller V/2fW, or different slip joint flow geometries that promote more eccentricity by static divergence.

There is little doubt that the entrance and exit bevels to the annular constriction of the original slip-joint (Fig. 1) are not the source of the self-excitation mechanism for upstream constrictions. Not only were critical velocities the same for annular constrictions with and without the bevels (Fig. 3), so were the flow damping (Figs. 4 and 5) and the pressure drop across the slip joint (Fig. 7). Note that this insensitivity to bevels must be restricted to the rather larger diffuser angle tested ($\sim 30°$), where flow separation is most likely fixed at the upstream edge of the bevel. Smaller angle bevels may indeed be the source of some unstable flow separation points and additional vibration self-excitation mechanisms.

Upstream constrictions with lengths in the range $6.25 < L/W' < 25.0$ had nearly the same critical velocities (Fig. 8), negative damping (Fig. 9), and pressure drop (Fig. 10) for $W'/W = 0.14$. This suggests, along with the critical velocity's insensitivity to the bevels, that the sudden changes in flow area caused by the constriction are alone responsible for the pressure drop and the vibration excitation mechanism of slip joints with upstream constrictions. In other words, a constriction formed with a very sharp-edged orifice would lead to similar critical velocities. However, this observed insensitivity to constriction length must be qualified to apply to the L/W' tested. Obviously, if L/W' becomes very large, the pressure drop due to friction losses in the constriction will dominate the pressure drop due to entrance and exit momentum losses. In such cases, the friction losses may become important to the self-excitation mechanism in more than one way. First the mechanism must be strong enough to overcome the increased initial (squeeze film) damping that accompanies an increased constriction length. Second, for a given pressure drop, the flow velocity through the slip joint will be decreased as the flow losses are increased. Thus, the critical velocity will be more difficult to attain. In fact, labyrinth seals, which increase flow losses, have been added as design fixes to reduce flow velocities below critical values [2].

D. Significant Design Variations

Previous testing [5] of the original slip joint geometry (Fig. 1 and Table 1), with significantly different amounts of initial damping in the fundamental mode showed that the larger initial damping could completely suppress self-excitation for some LD or, at least, increase the critical flow velocity. This is illustrated in the revised stability map shown in Fig. 15, where the solid lines define stability boundaries for each nominal value of fundamental mode damping. The slashes through a symbol indicate the flowrate where the instability ceased. The instability points for the second mode,

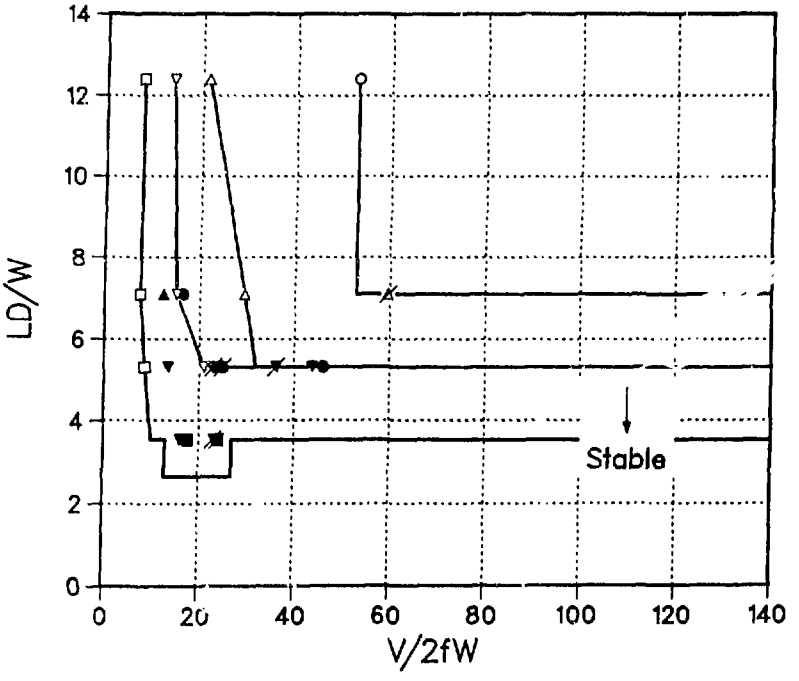

Fig. 15. Instability Map for Upstream Constriction of Original Slip Joint with Different Fundamental Modes ζ_o(%): 0.5, □; 2.2, ▽; 3.3, △; 6.6, ○

shown as solid symbols, tend to occur near the lower critical flow velocities of the first mode, which had the smallest nominal damping (~ 0.5%). Damping in the second mode was not controllable but was equally small (~ 0.3%), leading one to speculate the same mechanism was active in both modes. In any case, the solid line through the $\zeta_1 \sim 0.5\%$ points forms a stability boundary for all modes and damping tested. This stability boundary should be compared with the one in Fig. 3, which was obtained for an upstream constriction on the rigid tube (B in Fig. 2) instead of an upstream constriction on the flexible tube (A in Fig. 2 or Fig. 1). Even though the absolute flow directions are opposite, the similarity of the curves should be expected, assuming only the local details of the slip joint govern the self-excitation mechanisms.

The existence of the self-excitation mechanism depends greatly on the amount of tube engagement (overlap) beyond the constriction (LD ≠ 0). The greater the initial damping and the larger the constriction size, the larger the overlap LD must be for self-excitation to occur, as seen in Figs. 8, 12, and 15. However, once this non-zero threshold value is exceeded for a given system, the critical velocities for self-excitation do not vary much with increased LD. That is, the critical velocities are generally insensitive to variations in LD except in a very narrow range of borderline values marking the transition from a stable to an unstable configuration. In contrast, the flow damping varies almost monotonically with LD, decreasing for upstream

constrictions (Figs. 4, 9, and 13) and increasing for downstream constrictions (Figs. 5 and 11). The flow damping is important because it determines the forced vibration or the limit cycle vibration amplitudes. Thus, proper choice of LD could be used to limit vibration amplitudes for forced vibrations, particularly with downstream constrictions, or cases where self-excitation with upstream constrictions cannot be avoided.

The dependence of the upstream constrictions self-excitation mechanism on W' is as significant as the dependence on LD, and the dependences are interrelated as shown by the instability maps of Fig. 12 and the damping curves of Fig. 13. Just as a threshold value of LD exists for a given W', for a given value of LD a threshold value of W' exists below which instabilities can occur. Unlike the narrow band sensitivity to LD, the critical velocities vary monotonically with W' below the threshold value. The interdependence of W', LD, and V is very complex, as can be seen from the plots of flow damping in Fig. 13. Evidently, two damping mechanisms are active--one that produces negative damping and one that produces positive damping. The one producing negative damping appears to have a higher-order dependence on flow velocity, because maximums appear in the damping curves for some values of LD and W'.

The complex dependence of the flow damping $\zeta_1 - \zeta_o$ on the independent parameters $V/2f_1W$, LD, and W' shown in Fig. 13 were qualitatively predicted [8], as seen in Fig. 16, for a model problem sharing some geometric similarity to the slip joint. In the theory, the two-dimensional laminar flow equations for a very thin annulus are solved for centerbody motion of a rigid, circular rod of finite length LR in a circular channel that has a slightly larger diameter ($W/R \ll 1$). The rod has a constriction on its upstream end, which creates an annular orifice of width $W' < W$ and length $L = 0$, subject to the following assumptions: the entrance to the constriction does not create any pressure losses, the exit to the constriction is square, flow friction losses are negligible, and the flow acceleration boundary conditions can be derived from steady-state conditions. The downstream end of the rod is assumed tapered such that no flow losses are created. For these assumptions, the flow damping predicted for rigid body, transverse vibrations is

$$\zeta_1 - \zeta_o = \frac{\rho R^3}{M} \left(\frac{R}{W}\right) g(\varepsilon,\mu,\lambda) \tag{3}$$

and

$$g(\varepsilon,\mu,\lambda) = (\Pi/2\lambda)(1 - \operatorname{sech}\varepsilon)\left[\frac{2\mu - 1 + \mu\lambda^2(1 - \operatorname{sech}\varepsilon)}{1 + (\mu\lambda \tanh\varepsilon)^2}\right], \tag{4}$$

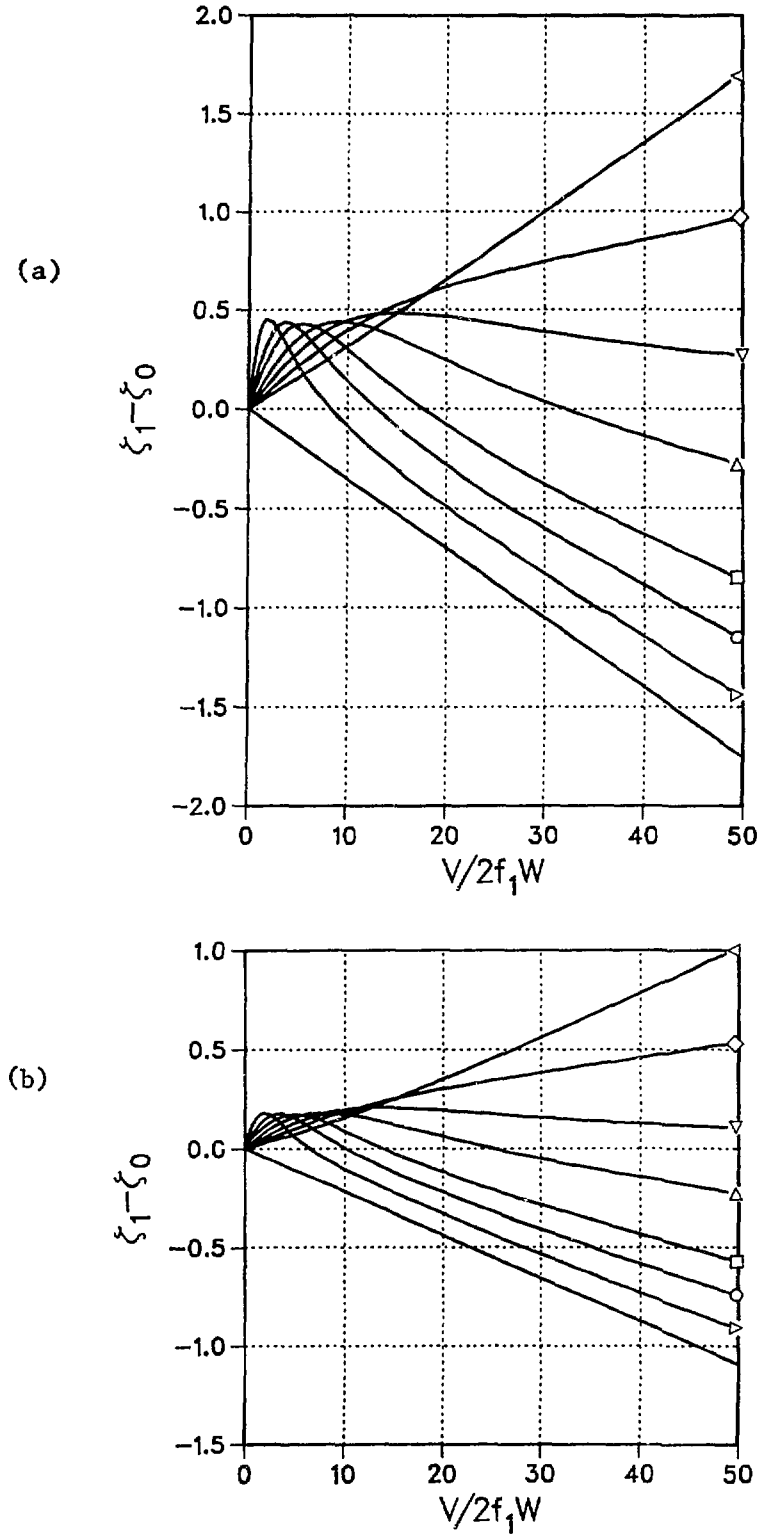

Fig. 16. Model Problem Predictions for Different W'/W (0.0, (——); 0.074, ▷; 0.14, ○; 0.21, □; 0.35, △; 0.50, ▽; 0.71, ◇; 1.0, ◁) and LD/W. (a) LD/W = 56.7, (b) LD/W = 14.18, (c) LD/W = 7.09

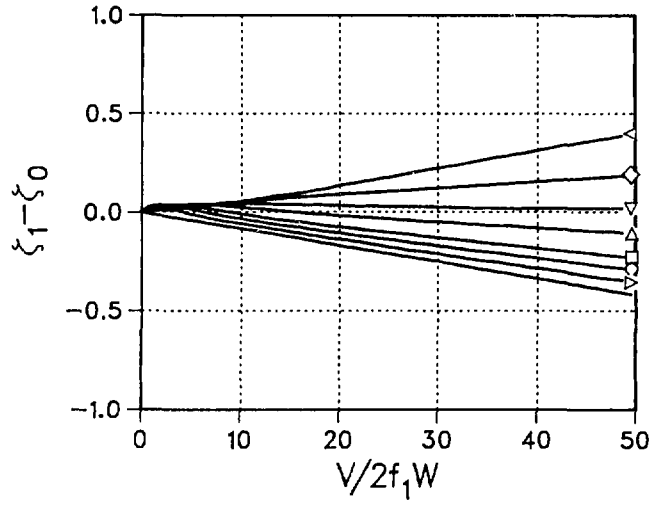

Fig. 16(c)

where R is the mean radius of the annulus between tubes, ρ is the fluid mass density, $\varepsilon = LD/R$, $\lambda = 2\pi(fR/V)$, $\mu = W'/W$, and M is the modal mass (deduced from [8] to be 1/2 the rigid body mass). Since $W/R \ll 1$, Eqs. 3 and 4 can be further reduced to

$$\zeta_1 - \zeta_o = \frac{1}{16}\frac{MF}{M}\frac{LD}{W}\frac{V}{2Wf}\, g_1(\mu,\alpha) \qquad (5)$$

and

$$g_1(\mu,\alpha) = \frac{2(2\mu - 1) + \mu\alpha^2}{1 + \mu^2\alpha^2}, \qquad (6)$$

where MF is the fluid mass in the large annulus and $\alpha = \pi(LD/W)(2Wf/V)$. Note that the parameters in Eqs. 5 and 6 are the same as those used to present the data for the slip joint. The predictions in Fig. 16 were determined with Eqs. 3 and 4 using the geometry of the slip joint, the mass density of room temperature water, and a rigid body end mass of 0.49 lb-sec^2/in. (86 kg). The end mass was determined using the measured natural frequency and the calculated stiffness of the flexible lower tube at the slip joint.

Many of the assumptions of the model problem do not match the conditions of the slip joint:

- Larger pressure losses are created by the less streamlined constriction of the slip joint,
- The slip joint constriction has a nonzero length,
- The flow losses at the exit from the annular region between the two tubes are not zero,
- The outside tube is flexibly mounted (not the center body), and
- Exposed surfaces of the outside tube extend both upstream from the constriction or downstream from the slip joint for many of the configurations tested.

Thus lack of quantitative agreement between Figs. 13 and 16 for LD/W = 14.18 and 7.09 is not surprising. Obviously, the slip joint tested produced much larger negative or positive flow damping and at a faster rate, with respect to the reduced velocity. The flow damping predictions for LD/W = 1.77 were not even shown for comparison to Fig. 13(c), because zero damping is predicted for all reduced velocities. Flow damping predictions for LD/W = 56.7, an annulus much larger than tested, are shown in Fig. 16(a) to illustrate the extremes necessary to predict damping magnitudes similar to those observed. Evidently the model problem mechanism is not as strong as that of the slip joint tested. Quite probably, the same theoretical approach would yield better correlation if the actual pressure losses of the slip joint's constriction were modeled [9]. Unfortunately, characterizing the pressure losses for annular constrictions is difficult and often direct measurement of critical velocities for self-excitation is just as easy.

E. Governing Dimensionless Parameters

The specific dimensionless parameters believed to control the self-excitation mechanism have been identified in the presentation of the data. Their choice is not necessarily obvious and was arrived at as testing progressed. A dimensional analysis of the slip joint of Fig. 1 would require that the governing independent dimensionless parameters include:

- A fluidelastic parameter,
- A fluid to solid mass ratio,
- Initial damping,
- Several length ratios defining the geometry of the slip joint, and

- A Reynolds number.

Also, although only qualitative comparisons can be claimed between the theory [8] and the experimental data, the theory of Eqs. 3 and 4 can be used to further refine the identity of the dimensionless parameters.

The reduced velocity V/2Wf was chosen as the fluidelastic parameter for the vibration mode with frequency f, where V is the average velocity in the annular constriction of width W'. The length scale used is 2W, the hydraulic diameter of the annulus between the tubes. Other combinations of velocity and length scales were investigated, such as V/2W'f. However, none of the other combinations identified the trends in both the instability map data (Fig. 12) and the flow damping data (Fig. 13), as well. The theory (Eqs. 3 and 4) suggests the length scale of the reduced velocity should be R, the radius of the annulus, instead of W. But for $W/R << 1$, Eqs. 3 and 4 can be rewritten in terms of a reduced velocity based on W, as shown in Eqs. 5 and 6. In any case, the trends of the data would not be changed because W/R was held constant for all tests.

The choice of $\zeta - \zeta_o$ as the dependent flow damping parameter was obvious, to eliminate the variations in initial modal damping ζ_o. Not only are the data reasonably ordered by use of $\zeta - \zeta_o$, but many of the tests repeated with significantly larger initial damping were found to overlap or form reasonable extrapolations of the data obtained with minimal initial damping. The solid symbols in Figs. 11(b), 11(c), and 14 were taken for $3.3\% \lesssim \zeta_o \lesssim 6.6\%$, whereas the rest of the data were for $\zeta_o \sim 0.5\%$. The theory in Eq. 3 only predicts flow damping (i.e., for $\zeta_o = 0$).

Since the self-excitation mechanism for an upstream constriction does not exist when the downstream annulus between the tubes is eliminated, the annular gap W and length LD are important parameters. The choice of the dimensionless parameter W'/W is a natural one because it is both a relative measure of the annular constriction width and the flow areas or hydraulic diameters of the two annular regions. For configurations where $W/D << 1$ is not a good approximation, an additional dimensionless parameter including D would be required. The dependence on W/D may not be like that given in Eqs. 3 and 4, because their derivation assumed $W/R << 1$.

For three reasons, the length LD of the annulus between tubes is more fundamental in influencing the self-excitation mechanism of upstream constrictions than the total engagement length IL = LD + 2BL + L.

- LD must be greater than zero for self-excitation, and changes in BL and L have been found to have no effects on the instabilities.

- For the same LD/W, critical flow velocities and negative $\zeta_1 - \zeta_o$ are similar for different length constrictions (Figs. 8 and 9).
- For the same LD/W, the flow damping $\zeta_1 - \zeta_o$ is similar for tests with and without leading and trailing bevels to the annular constriction (see Figs. 3, 4, and 5).

The similarity of the damping curves is a much better justification for choosing LD/W than the similarity of instability maps, because the critical velocities, as explained previously, are generally insensitive to variations in LD/W or IL, except in the very narrow range of borderline values around the threshold value of LD/W required for transition from a stable to an unstable flow geometry. In contrast, flow damping is generally sensitive to all variations in both LD/W and flow velocities V/2fW. The theory [8] assumes BL = L = 0, but LD/W appears prominently in Eqs. 5 and 6.

The sensitivity of the self-excitation mechanism was not tested explicitly for Reynolds number dependence. The test temperature of the water flow was maintained in the range 16-26°C for all testing to avoid significant changes in flow channel friction factors. The fact that the pressure drop was not significantly affected by changes in the constriction length suggests that Reynolds numbers is not important for the flow geometries tested. However, many leakage flow self-excitation mechanisms depend on Reynolds number [2].

Since fluid and structural properties were held constant throughout testing, the mass ratio dependence could not be assessed experimentally. But Eqs. 3-6 clearly show that flow damping depends directly on the ratio of fluid to structural mass.

F. Second Mode Instabilities

When testing of upstream constrictions first began [4], it was questionable whether the second-mode vibrations could be self-excited. In particular, the fluid forces produced in the downstream annulus act at the antinode for the first cantilevered mode, an effective location for excitation forces. But the same annulus is very near the node of the second cantilevered mode, an ineffective location. Somewhat surprisingly, a second-mode instability was observed (Fig. 15) for the original slip joint (Fig. 1) when the first-mode instability was suppressed by large ζ_o or small LD. In fact, weak instabilities were observed in the lighter damped second mode at LD too small to produce first-mode instabilities. The excitation mechanism is thought to be the same for both modes, because the critical reduced velocities for the second mode were in the same range as those of the first mode when the initial damping was similar. This similarity even existed when the bevels were removed (Fig. 3) or the constriction length was shortened (Fig. 8). Also,

these observations are strong justifications for the use of the reduced velocity V/2fW as the fluid elastic parameter, because the difference in the fundamental and second-mode frequencies is significant: 3.1 versus 21.1 Hz.

The fact that few pure second-mode instabilities were observed for the shorter constriction lengths L/W' = 6.25 and 12.5 (Figs. 8 and 12) can be explained. Most important, the fundamental mode mechanisms were stronger for shorter constrictions, and tube-to-tube impact usually occurred before a pure second mode could be excited. A switch to the second or hinged mode often occurred with tube-to-tube impact, but this was not recorded as a second-mode instability because of the presence of the impact forces. In all but one of the cases where a fundamental mode instability ceased and the presence of second mode self-excitation could be investigated, the engagement length was very short (LD/W = 4.43). Thus, second-mode self-excitation was only observed when the mechanism was strongest (W'/W = 0.08). In the one case where first-mode instability ceased at a significantly long engagement length (LD/W = 7.09), a second-mode self-excitation was observed for a W'/W as large as 0.28.

In summary, self-excitation of second and higher modes of vibration cannot be ruled out even when the slip joint is near an antinode of the mode, especially since higher modes are usually more lightly damped. The exact conditions for self-excitation in higher modes would be difficult to determine experimentally because of the infinite combinations of rotational and translational motion possible at the slip joint. However, curves bounding the stable parameter ranges for fundamental mode self-excitation at minimal ζ_o appears to bound the self-excitation conditions in the second mode.

VI. DESIGN RULES

For the original slip joint geometry (Fig. 1 and Table 1), self-excitation due to leakage flow can be avoided by maintaining

- A downstream flow constriction,
- An annulus length LD/W < 3, or
- V/2fW < 5.

Also, these design rules are valid for concentric or fully eccentric tube alignments, when the exit and entrance bevels are removed, when the annular constriction gap is made larger, or when the constriction length is shortened, with one exception for downstream constrictions:

- For L/W' < 25, maintain IL > 0.2 D.

These rules for avoiding instabilities are relatively simple and easy to realize.

Downstream constrictions can be created for the slip joint of Fig. 1 by reversing the flow direction. If the flow direction cannot be reversed, then the constriction can be moved to the bottom of the rigid tube to achieve the same effect. If the constriction and flow direction must remain as shown in Fig. 1, then self-excitation can be avoided by shortening the engagement length LD to less than 3 W. If short engagements are not possible, then several other possibilities exist to satisfy $V/2fW < 5$. The easiest are to increase W or reduce V, perhaps by increasing W'. Raising the fundamental frequency f usually is not a feasible alternative, but must not be discounted. If the design constraints do not allow any of these many modifications, which would be surprising, design rules can be formulated from Figs. 12, 14, and 15 that are more complicated and difficult to realize.

The restrictions on the reduced velocity can be relaxed if W'/W can be increased to satisfy $V/2fW < 50\ W/W'$. If the reduced velocity condition cannot be satisfied, but W'/W can be increased, then avoidance of self-excitation is still possible if LD/W can be made to satisfy one of the following conditions:

- $LD/W < 4$ with $W'/W \geq 0.30$,
- $LD/W < 7$ with $W'/W \geq 0.35$, or
- $LD/W < 14$ with $W'/W \geq 0.50$.

If none of these conditions can be met, then the damping in all the modes must satisfy:

- $\zeta_o \geq 1/2\%$ for $V/2fW < 7$ or $LD/W < 3$,
- $\zeta_o \geq 2\%$ for $V/2fW < 13$ or $LD/W < 5$,
- $\zeta_o \geq 3\%$ for $V/2fW < 20$ or $LD/W < 5$,
- $\zeta_o \geq 4\%$ for $V/2fW < 30$ or $LD/W < 5$, and
- $\zeta_o \geq 6\%$ for $V/2fW < 50$ or $LD/W < 7$.

Usually, changing the damping or structural frequencies in existing designs is very difficult.

VII. CONCLUSIONS

Testing of many variations of the original slip joint design of Fig. 1 has shown that the entrance and exit bevels to the constriction can be removed (BL = 0.0) and the constriction length L shortened without significantly changing the critical flow velocities V/2fW at which vibration of the lower tube is self-excited. In addition, reducing the size of the constriction W', relative to W, decreased the strength of the mechanism and the likelihood of self-excitation. The effects of changing W' were similar to those observed in the past when the engagement length LD was made smaller, including complete suppression of the mechanism when $W'/W > 0.5$. These observations point to a mechanism that depends primarily on the discontinuity in flow areas caused by the constriction. Similar results could be expected for a sharp-edge orifice. This supposition is strengthened by the observation that the pressure drop across the slip joint was not significantly affected by the changes in the bevels or constriction lengths.

Tests at constriction lengths less than, or equal to, half the original length (Table 1), revealed a self-excitation mechanism that does not require an annular region downstream from the constriction. Not a lot was learned about the mechanism, but it was only active for total engagement lengths IL less than 20% of the diameter of the rigid tube. Since such small engagements are easy to avoid in practice, further investigation was not necessary to produce design rules, but further work is planned to identify the character of the mechanism.

The extensive identification of critical velocities reported here for variations in flow damping, constriction length L, and the constriction gap size W', combined with previous work, has provided a data base from which comprehensive design rules could be formulated to avoid self-excitation by leakage flow. Two very simple design rules to avoid self-excitation due to leakage flow through the slip joint are:

- Use a downstream constriction with an engagement length greater than 20% of the annulus diameter, and
- Use an upstream constriction only when the downstream annulus length is less than three widths of the radial gap between the two tubes.

Alternative design rules are given in Section VI which are not as easy to apply and realize.

ACKNOWLEDGMENTS

This work was performed under the sponsorship of the Office of Reactor Research and Technology, U.S. Department of Energy.

The author is grateful to Roger Smith for his help in performing the flow tests. Also, the test program guidance and interpretation of results by Marty Wambsganss are much appreciated.

REFERENCES

1. M. P. Paidoussis, "Flow-Induced Vibration in Nuclear Reactors and Heat Exchangers: Practical Experiences and State of Knowledge," in Practical Experiences with Flow-Induced Vibrations (E. Naudascher and D. Rockwell, eds.), Springer-Verlag, New York, pp. 1-81 (1980).

2. T. M. Mulcahy, "Leakage Flow-Induced Vibrations of Reactor Components," The Shock and Vibration Digest 15(9), 11-18 (1983).

3. M. W. Parkin, "Flow-Induced Vibration Problems in Gas Cooled Reactors," in Practical Experiences with Flow-Induced Vibrations (E. Naudascher and D. Rockwell, eds.), Springer-Verlag, New York, pp. 126-136 (1980).

4. T. M. Mulcahy, "Leakage Flow-Induced Vibration of a Tube-in-Tube Slip Joint," Symposium on Flow-Induced Vibration; Volume 4, Vibration Induced by Axial and Annular Flows (M. P. Paidoussis and M. K. Au-Yang, eds.), ASME, New York, pp. 15-24 (1984).

5. T. M. Mulcahy, "Avoiding Leakage Flow-Induced Vibration by a Tube-in-Tube Slip Joint," Argonne National Laboratory Report, ANL-84-82, Argonne, IL (1984). Also in Fluid-Structure Interaction and Aerodynamic Damping, ASME, New York, Sept. 1985, pp. 159-169.

6. T. M. Mulcahy, "Leakage Flow-Induced Vibration of an Eccentric Tube-in-Tube Slip Joint," Argonne National Laboratory Report, ANL-85-56, Argonne, IL (1985).

7. D. R. Miller, "Generation of Positive and Negative Damping with a Flow Restrictor in Axial Flow," Proceedings of the Conference on Flow-Induced Vibrations in Reactor System Components, Argonne National Laboratory, ANL-7685, pp. 304-307 (May 1970).

8. D. E. Hobson, "Fluid-Elastic Instabilities Caused by Flow in an Annulus," Presented at the 3rd Conference on Vibrations in Nuclear Plant, May 11-14, 1982, Keswick, English Lakes, U.K.

9. A. Spur and D. E. Hobson, "Forces on the Vibrating Centrebody of an Annular Diffuser," Symposium on Flow-Induced Vibration; Volume 4, Vibration Induced by Axial and Annular Flows, ASME, New York, pp. 41-52 (1984).

Distribution for ANL-86-11

Internal:

C. E. Till
R. S. Zeno
P. R. Huebotter
M. W. Wambsganss
S. S. Chen
H. Halle
J. A. Jendrzejczyk
T. M. Mulcahy (20)
H. H. Chung
W. P. Lawrence
S. K. Zussman
R. A. Valentin
R. A. Lewis
Y. I. Chang
D. J. Malloy
R. W. Seidensticker
ANL Patent Dept.
ANL Contract File
ANL Libraries (2)
TIS Files (5)

External:

DOE-TIC, for distribution per UC-79k (114)
Manager, Chicago Operations Office, DOE
Director, Technology Management Div., DOE-CH
E. Gallagher, DOE-CH
Director, FFTF/PO
Manager, Engineering Technology Department, FWEC (2)
M. K. Au-Yang, B&W
E. B. Baumeister, Rocketdyne Div.
M. D. Bernstein, FWEC
C. C. Bigelow, DOE/Nuclear Energy
R. D. Blevins, GA
J. C. Blomgren, Commonwealth Edison
G. J. Bohm, W
S. J. Brown, QED
C. C. Chamis, LeRC/NASA
C. A. Chandley, TVA
S. Chandra, Northeast Utilities
P. Y. Chen, NRC
J. M. Chenoweth, HTRI
H. J. Connors, W R&D
J. Corr, Saratoga, CA
W. K. Da..n, MSFC/NASA
A. Dalcher, GE-ARSD
E. H. Dowell, Duke Univ.
W. Edelstein, IIT
R. J. Fritz, GE/KAPL
E. L. Gluekler, GE
O. K. Goetz, MSFC/NASA
N. Grossman, DOE/Nuclear Energy
J. E. Haas, LeRC/NASA
R. J. Hansen, NRL
M. Hartzmann, NRC/NRR
R. A. Johnson, Rocketdyne Div.
S. P. Kalra, EPRI
E. Kiss, GE
B. T. Lubin, CE
K. McConnell, Iowa State U.

E. Moody, Rocketdyne Div.
R. J. Neuhold, DOE/Nuclear Energy
E. H. Novendstern, W-Nuclear Fuel Div.
E. E. Olich, GE
P. R. Pluta, GE
L. Povinelli, LeRC/NASA
J. Rajan, NRC
M. M. Reischmann, ONR
E. L. Reiss, Northwestern Univ.
B. J. Rock, DOE/Nuclear Energy
J. A. Ryan, HEDL
J. B. Sandifer, B&W/ARC
S. D. Savkar, GE/CRD
M. Sax, W-Bettis
J. Schwab, LeRC/NASA
J. C. Simonis, Southwest Res. Inst.
N. R. Singleton, W
D. Steininger, EPRI
H. Struck, MSFC/NASA
M. R. Torres, GE
R. Volin, Shock & Vibration Center
G. H. Weidenhamer, NRC/RES
F. R. Wiltshire, GE
T. M. Yang, GE-ARSD
E. A. Zanoni, W/Bettis

Components Technology Division Review Committee:
P. Alexander, Flopetrol Johnston Schlumberger, Houston
D. J. Anthony, General Electric Co., San Jose
A. A. Bishop, U. Pittsburgh
B. A. Boley, Northwestern U.
R. N. Christensen, Ohio State U.
R. Cohen, Purdue U.
R. E. Scholl, URS, San Francisco
J. Weisman, U. Cincinnati